3rd IAHR International Meeting of the Workgroup on Cavitation and Dynamic Problems in Hydraulic Machinery and Systems, October 14-16, 2009, Brno, Czech Republic

NUMERICAL SIMULATION OF NONLINEAR SELF-OSCILLATIONS OF A FULL LOAD VORTEX ROPE

Sébastien.Alligné*
Laboratory for Hydraulic Machines, EPFL Lausanne, Switzerland
Christophe Nicolet
Power Vision Engineering sàrl, Ecublens, Switzerland
Nicolas Ruchonnet
Laboratory for Hydraulic Machines, EPFL Lausanne, Switzerland
Vlad Hasmatuchi
Laboratory for Hydraulic Machines, EPFL Lausanne, Switzerland
Pierre Maruzewski
Laboratory for Hydraulic Machines, EPFL Lausanne, Switzerland
François Avellan
Laboratory for Hydraulic Machines, EPFL Lausanne, Switzerland

ABSTRACT

Self excited instabilities or oscillations of a cavitating full load vortex rope occur due to an interaction between the gas volume and the acoustic waves. From the onset of the oscillations, the amplitudes grow until they reach a maximum, called the “limit cycle”. The aim of this paper is to predict and to simulate this full load instability with its corresponding “limit cycle”. The test case is a reduced scale model installed on test rig in the Laboratory for Hydraulic Machines at the EPFL. An advanced hydro acoustic vortex rope model is developed to take into account the energy dissipation due to thermodynamic exchange between the gas and the surrounding liquid. Three key hydro acoustic parameters are set up using both steady CFD simulations and analytical models. First of all, parameters are assumed to be constant and time domain simulation is divergent without reaching the limit cycle. However frequency of instability is well predicted. Then inclusion of nonlinear parameters is found to lead to a limit cycle of finite amplitude. Prediction is compared with results from experiments and is in good agreement. It is shown that nonlinearity of the viscoelastic damping parameter, modelling the energy dissipation, is decisive to reach the limit cycle. Moreover, an energy approach is developed to understand the interaction process between the mass source and the system dissipation to reach the equilibrium at the limit cycle. It brings out that over one period the dissipation can provide energy to the system whereas the mass source dissipates to ensure the equilibrium.

KEYWORDS

Nonlinear self oscillations, viscoelastic damping, vortex rope, instability, eigenvalues.

* *Corresponding author:* Laboratory for Hydraulic Machines.,av. De cour 33 bis,CH 1007 Lausanne, Switzerland, phone: +41 216937381, fax: +41 216933554, email: sebastien.alligne@epfl.ch

1. INTRODUCTION

The growing development of renewable energies combined with the process of privatization, lead to a change of the economical energy market strategies. Instantaneous pricings of electricity as function of the demand or the predictions, induces profitable peak productions which are mainly covered by the hydroelectric power plants. Therefore, the operators harness more and more hydroelectric facilities at full load operating conditions. However, Francis Turbine features an axisymetric rope leaving the runner which may acts under certain conditions as an internal energy source leading to instability. Undesired power and pressure fluctuations are induced and prevent to take advantage of the maximum available power.

Koutnik and Pulpitel [1] applied to Francis Turbines the modelling approach developed initially for pump stability analysis based on the use of the cavitation compliance C and of the mass flow gain factor χ parameters, see Brennen and Acosta in 1973 [2] and 1976 [3]. Using the transfer matrix method, Koutnik and Pulpitel [1] derived a stability diagram to explain a full load surge occurring on a four 39MW Francis Turbine power plant. A similar approach based on cavitation parameters mapping was also successfully applied to explain inducer instabilities by Tsujimoto et al. in 1993 [4] and propeller instabilities by Duttweiler and Brennen in 2002 [5] and by Watanabe and Brennen in 2003 [6]. More recently, deriving the compliance and the mass flow gain factor parameters from CFD simulations of the complete machine, Flemming et al [7] predicted instability of a prototype installation based on eigenvalues and eigenmodes analysis. However, no validation was available. These stability analyses based on constant hydro acoustic parameters C - χ allows to predict frequencies and mode shapes. However, this method does not give any information about the amplitude of the oscillations. In 2006, Koutnik et al. [8] performed a time domain simulation of a self oscillation occurring in a four 400MW Francis Pumped-Storage plant. In order to obtain finite fluctuations called “limit cycle”, nonlinearity on the cavitation compliance as function of the Thoma number is introduced. Moreover, the system is pushed to the limit of the instability by setting a mass flow gain factor parameter very low compared to the one derived from the stability analysis. Therefore, during the transient, the system enters in unstable conditions and nonlinearity of the compliance switches between stable and unstable conditions allowing to reach the limit cycle. It has been shown by authors that limit cycle is reachable only if nonlinearity of hydro acoustic parameters is taken into account.

The aim of this paper is to predict and simulate the instability phenomenon with its corresponding limit cycle without being at the edge of the instability. The test case is a reduced scale model installed on test rig in the Laboratory for Hydraulic Machines at the EPFL. For large guide vane openings, instability occurs and the cavitating vortex rope experiences volume pulsations as described in Section 2. The best known mechanism of self oscillation excitation is so called negative friction [9]. Considering a spring-mass system with a damper in parallel, the self oscillation mechanism is driven by a linear equation of the following form:

$$m \cdot \ddot{x} + c \cdot \dot{x} + k \cdot x = 0 \tag{1}$$

When the damping c is negative, instead of energy being lost due to the friction, energy is generated within the system. A slight disturbance from equilibrium leads to the system being carried far from the equilibrium state without reaching a limit cycle. However, if a nonlinear damping is introduced the limit cycle is reachable. The well known mechanical system is the Kaidanovsky-Khaikin frictional model [9] [10] which consists of a mass m fixed to a wall by a spring and lying over a transmission belt moving with a given velocity. The nonlinear dry friction force on the belt can under certain conditions induce negative friction. Inspired by these mechanical models, a new vortex rope model is developed in Section 3 by adding dissipation to the standard C- χ model used in the literature. The proposed dissipative model

is based on the work of Pezzinga [11] who developed an analytical model of dissipation in cavitating pipe flows due to thermodynamic exchange between the gas and the surrounding liquid. In this new model, three key hydro acoustic parameters must be set up: the compliance, the mass flow gain factor and the dissipative term called the viscoelastic damping. As a first step, constant parameters are considered and computed from steady CFD simulations of the complete machine. A stability analysis by means of eigenvalues and eigenmodes computation is performed to confirm the instability of the investigated operating point in Section 4. The corresponding time domain simulation is performed in Section 5 whereas in Section 6 nonlinear parameters are used. Results of simulations will be compared to the experimental "limit cycle".

2. EXPERIMENTAL MEASUREMENTS ON TEST RIG

A full load instability phenomenon occurred for a reduced scale model installed on a test rig at the Laboratory for Hydraulic Machines. Pressure measurements synchronized with high speed video camera have been used to monitor the instability. At the unstable operating point, the cavitating vortex rope experienced volume pulsations as shown in Fig. 1.

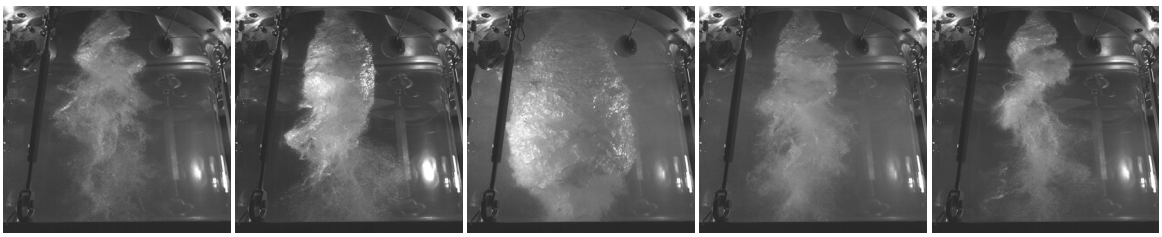

Fig.1 Vortex rope pulsation at the unstable operating point

The corresponding time history and frequency spectra of pressure fluctuations in the cone are given respectively in Fig.2 a) and Fig.2 b).

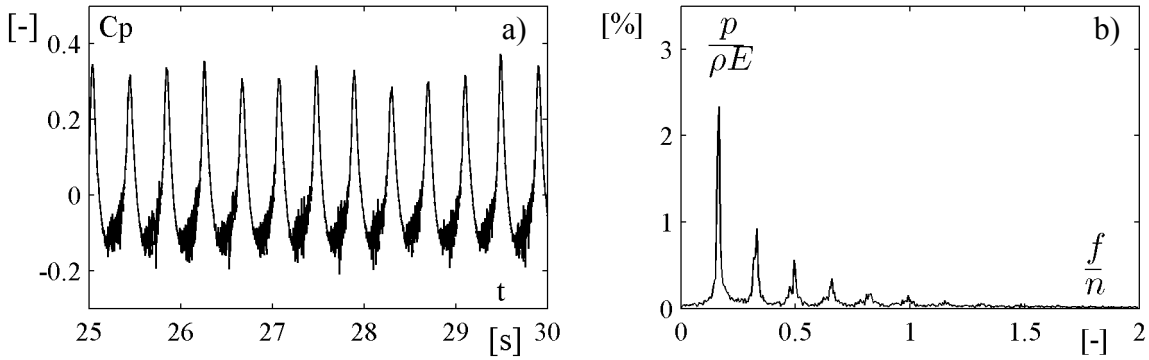

Fig.2 a) Time history and b) frequency spectra of pressure fluctuations in the cone

The unstable frequency of pressure signals is $f = 2.5$ Hz which corresponds to the vortex rope pulsation. The aim of this paper is to perform a hydro-acoustic numerical simulation which brings out the unstable frequency and the typical time signal's shape.

3. SETUP OF THE HYDROACOUSTIC MODEL

Hydroacoustic model

The test rig and the investigated reduced scale model have been implemented in the hydro-acoustic SIMSEN software. Initially, SIMSEN was developed by the EPFL for the transient and steady-state simulation of electrical power systems and control devices having an

arbitrary topology. Then, the capability of the software was extended to hydraulic components in order to be able to simulate the transient behaviour of a complete hydroelectric power plant. The most common hydraulic components have been implemented such as pump-turbine, penstock, surge tank, gallery, valve, reservoir, etc [12]. In order to get a common set of differential equations for both electrical and hydraulic parts, hydraulic models are based on an electrical analogy. Fig.3 gives an overview of the implemented SIMSEN model of the test rig which is a closed loop system with one reservoir and one feed pump.

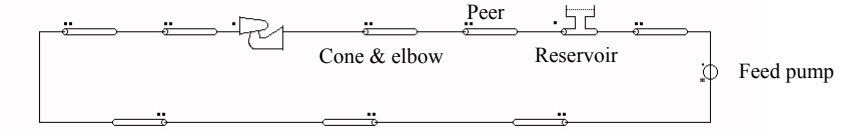

Fig.3 SIMSEN model layout

Modelling of the wave propagation in the pipes is a decisive issue to be able to predict and simulate an instability phenomenon. The viscoelastic behaviour for both fluid and wall material must be taken into account in the pipe model to predict accurately pressure fluctuations amplitudes and system stability limits, [13]. The equivalent electrical scheme of a standard viscoelastic pipe, derived from continuity and momentum balances, can be represented as a T-shaped RLC circuit, see [12]. On the other hand, because of the onset of the cavitating vortex rope in the draft tube, this component cannot be modelled like a standard viscoelastic pipe. Indeed, the cavitation modifies the continuity equation of the standard viscoelastic pipe model. As shown in Fig. 4 a), the draft tube is divided in two parts. Assuming the cavitation located in the cone and the elbow parts between sections $\bar{1}$ and $\bar{2}$, the equivalent electrical scheme is given in Fig. 4 b).

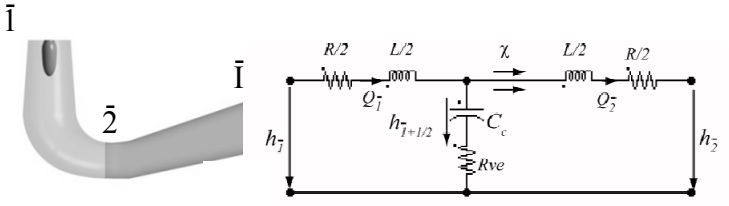

Fig.4 a) Draft tube domain and b) equivalent electrical scheme of the set of cone and elbow parts

In the framework of this investigation, the cone and the elbow are modelled with one pressure node and the corresponding continuity equation, modified by the cavitation, is:

$$Q_{\bar{1}} - Q_{\bar{2}} = \frac{DV_c}{Dt} = C_c \frac{dh_{\bar{1}+1/2}}{dt} + \chi \frac{dQ_{\bar{2}}}{dt} \tag{2}$$

The discharge variation is equal to the variation of the cavitation volume V_c which is function of two state variables: the head and the discharge, [2], [3]. C_c and χ are respectively the cavitation compliance and the mass flow gain factor defined as:

$$C_c = -\frac{\partial V_c}{\partial h_{\bar{1}+1/2}} = \frac{g \cdot A \cdot L}{a^2} \qquad \chi = -\frac{\partial V_c}{\partial Q_{\bar{2}}} \tag{3}$$

The onset of the cavitating vortex rope induces:

- a change of the wave speed a in the cone and the elbow [14], [15] which in turns modifies the cavitation compliance C_c according to Eq. 3,
- the appearance of the mass flow gain factor parameter which represents the excitation mass source of the hydraulic system being defined as the cavitation volume variation as function of a discharge variation.

Moreover, a third parameter of the equivalent electrical scheme is modified by the cavitation: the equivalent viscoelastic damping μ_{equ} which defines the viscoelastic resistance in serie with the capacitance according to Eq. 4.

$$R_{ve} = \frac{\mu_{equ}}{A \cdot \rho \cdot g \cdot L} \tag{4}$$

The viscoelastic damping μ_{equ} of both fluid and wall material decreases when cavitation appears. This parameter allows to model the energy dissipation due to thermodynamic exchange between liquid and gas [11]. For more clarity, the model of the set cone and elbow will be called further as the vortex rope model.

Computation of the hydro-acoustic vortex rope model parameters

The RLC model parameters of the standard viscoelastic pipes without cavitation are computed from the hydro acoustic characteristics of each component, [12]. However, the computation of the three key parameters of the vortex rope model such as the wave speed, the mass flow gain factor and the equivalent viscoelastic damping, is performed by CFD simulations of the three dimensional flow, [7] with the commercial simulation software ANSYS CFX 11.0. Incompressible RANS steady simulations are performed with the Shear Stress Tensor turbulence model. Moreover, single phase simulations are considered. Therefore, to derive the hydro-acoustic parameters, the cavitation vortex rope volume is assumed to correspond to the flow region bounded by the vapour pressure p_v set to 2338 Pa at 20°C. In order to compute the three parameters corresponding to the investigated unstable operating point showed in Section 2, boundary conditions of the computational domain are setup according to experimental data. The Thoma number and discharge measurement allow to define respectively the outlet pressure and the inlet velocity of the computational domain. Since steady CFD simulations are performed, the cavitation compliance can be computed as the vortex rope volume variation as function of the outlet head $h_{\bar{I}}$ variation of the computational domain or the Thoma number, see Eq. 5.

$$C_c = -\frac{\partial V_c}{\partial h_{\bar{I}+1/2}} = -\frac{\partial V_c}{\partial h_{\bar{I}}} = -\frac{1}{H}\frac{\partial V_c}{\partial \sigma} \tag{5}$$

Fig. 5 shows the vortex rope volume as function of the Thoma number variation.

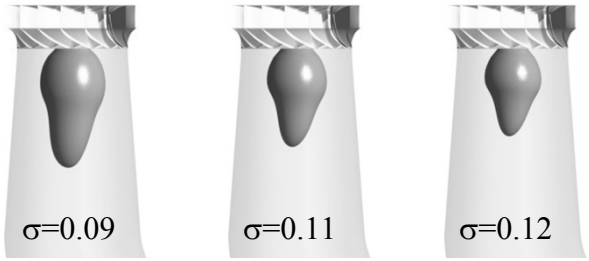

Fig.5 Variation of the vortex rope volume as function of the Thoma number

The central finite difference approximation leads to a compliance value of $C_c = 0.0024$ m^2 corresponding to a wave speed of $a = 27$ m.s^{-1} for the experimental Thoma number of $\sigma = 0.11$.

On the other hand, the mass flow gain factor, is computed as the vortex rope volume variation as function of the discharge variation, see Fig. 6.

Fig.6 Variation of the vortex rope volume as function of the discharge

The central finite difference approximation leads to a mass flow gain factor value of $\chi = -0.033$ s at the experimental investigated discharge Q_n. The last parameter to derive from CFD simulations is the equivalent viscoelastic damping. This parameter models the energy dissipation in unsteady cavitating flows due to a combination between the gas release and the heat exchange between the gas and the surrounding liquid. Considering both effects and assuming an homogeneous cavitation in the pipe cross section, Pezzinga [11] developed a formulation for the second viscosity as follows:

$$\mu_{equ} = \frac{\Theta \cdot \rho_c \cdot R \cdot T \cdot \rho_m^2 \cdot \alpha_c \cdot a^4}{p^2} \tag{6}$$

Of course, the vortex rope volume at full load conditions is far from the assumption of an homogeneous cavitation development in the pipe. However, this parameter being unknown for the vortex rope model, this formulation is considered as a first approximation to get an order of magnitude of this parameter. To derive this parameter from CFD simulations, pressure is considered at the outlet of the CFD domain; wave speed and cavitation volume, have been computed previously. By applying this expression at the operating point defined by the Thoma number $\sigma = 0.11$ and the investigated discharge Q_n, it yields to an equivalent viscoelastic damping value of $\mu_{equ} = 1555$ Pa.s. Tab. 1 summarizes the three key hydro-acoustic parameters derived from CFD simulations.

a [m.s^{-1}]	χ [s]	μ_{equ} [Pa.s]
27	-0.033	1555

Tab.1 Hydro-acoustic parameters of the vortex rope model derived from CFD simulations

4. STABILITY ANALYSIS OF THE OPERATING POINT

In SIMSEN, dynamic behavior of the hydro-acoustic model of the test rig is given by a set of first order nonlinear differential equations of the following form:

$$[A] \cdot \frac{d\vec{X}}{dt} + \left[B\left(\vec{X}\right)\right] \cdot \vec{X} = \vec{V}\left(\vec{X}\right) \tag{7}$$

where $[A]$ and $\left[B\left(\vec{X}\right)\right]$ are the state global matrices of dimension $[n \times n]$, $\vec{X}$ and $\vec{V}\left(\vec{X}\right)$ are respectively the state vector and the boundary conditions vector with n components. The equations of the vortex rope model developed in Section 3 are included in this matrix system. And the three vortex rope parameters are considered as constant for the stability analysis, see Tab.1.

Nonlinearity of this system is due to [13]:

- the resistance terms in matrix $\left[B\left(\vec{X}\right)\right]$ modeling the head losses in the pipes;
- the Francis Turbine component modeled by a nonlinear pressure source in the boundary vector $\vec{V}\left(\vec{X}\right)$.

Stability analysis in SIMSEN [13] is based on linearization of this set of equations around an equilibrium point and then, stability is deduced from eigenvalues of the linearized set of differential equations. Damping and oscillation frequency of the eigenmodes are respectively given by the real part and the imaginary part of the eigenvalues. If the real part is negative the mode is stable, whereas if it is positive the mode is unstable. Moreover, each eigenvalue is associated to an eigenvector which represents the eigenmode's spatial shape. For the vortex rope parameters given in Tab.1 eigenvalues and eigenvectors are computed. In Fig. 7 the first five eigenvalues are plotted in the complex plan. The x-axis corresponds to the modal damping and the y axis to the modal frequency.

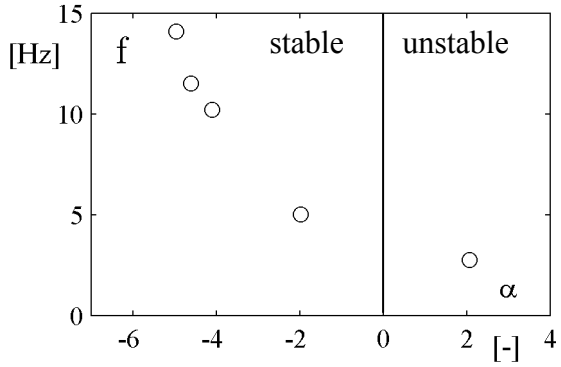

Fig.7 System eigenvalues with parameters given in Tab. 1

The unstable eigenmode corresponding to a positive modal damping, is the first eigenmode which frequency is $f = 2.7$ Hz. Therefore, using the parameters derived from CFD simulations, the unstable frequency of the vortex rope pulsation is predicted with an error of 8% according to the experimental value of 2.5 Hz. Moreover, this result shows that the unstable frequency measured experimentally in the cone corresponds to the first eigenmode of the system which is plotted in Fig. 8.

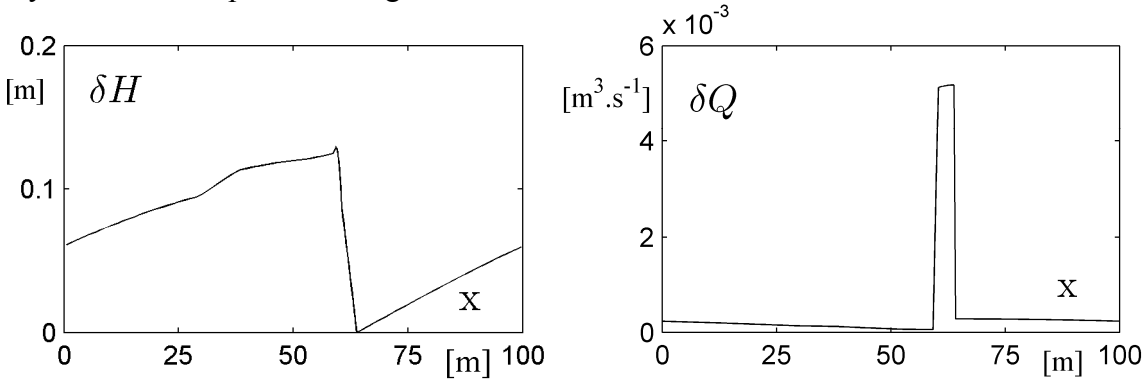

Fig.8 First eigenmode unstable: a) pressure δH and b) discharge δQ fluctuations

The x axis is the abscissa representing the location in the test rig. Being a closed loop system, abscissa $x = 0$ m and $x = 100$ m corresponds to the same location, being the feed pump location. The draft tube component is located between $x = 59$ m, the runner outlet location, and $x = 64$ m, the downstream reservoir location. One can observe that the standing wave in the test rig, features large discharge fluctuations due to the vortex rope large compliance compared to the pipes and the related large vapor volume fluctuations during the oscillations.

The linearization of the set of differential equations allows to identify the system stability and predicts sytsem eigenfrequencies and related mode shapes. However, this method does not give any information about the amplitude of the oscillations. Indeed, this linear theory only predicts that the amplitude of the eigenmode fluctuations given in Fig.8 grow exponentially in time according to the modal damping given in Fig. 7. The aim of this paper is to simulate in the time domain pressure and discharge fluctuations of the standing wave which should grow exponentially until a maximum, called a "limit cycle".

5. NUMERICAL SIMULATION WITH CONSTANT MODEL PARAMETERS

In this Section, time domain simulation of the instability is performed with constant vortex rope parameters given in Tab. 1. Time history of pressure fluctuations at the node of the vortex rope model is given in Fig. 9.

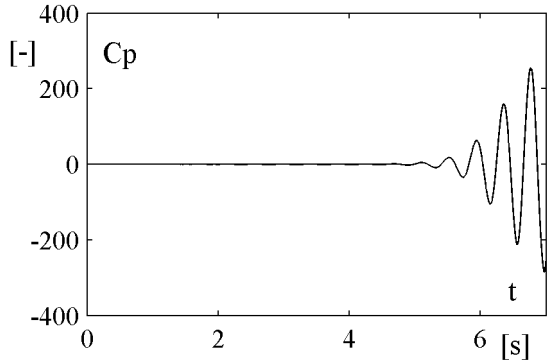

Fig.9 Time history of pressure fluctuations in the draft tube

One can observe that the simulation is divergent which induces very high pressure fluctuations without reaching a "limit cycle". In accordance with the eigenvalue analysis, the unstable frequency simulated in the time domain is $f = 2.7$ Hz. In the field of mechanical oscillations, a typical representation, called a "phase plane", is extensively used to obtain properties of the differential equations such as equilibrium, periodicity or stability. Usually, for hydro-acoustic systems, the phase plane represents the pressure as function of the discharge [16] and the resulting curve is called the phase path. In Fig. 10 pressure of the vortex rope model as function of the outlet discharge is plotted to represent the phase plane of the simulation.

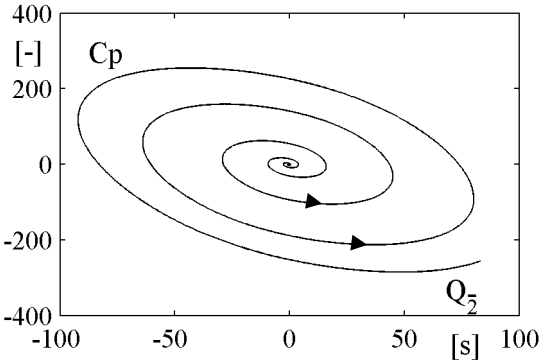

Fig.10 Phase plane diagram

By definition, a "limit cycle" is an isolated periodic solution of the system [17] and is represented in the phase plane by an isolated closed path. During one period along the closed path, the total energy of the system ξ returns to its original value, see Eq. 8.

$$\xi\left(T\right) - \xi\left(0\right) = 0 \tag{8}$$

In that case, the energy loss in the system and the energy gain of the vortex rope excitation are at equilibrium. Since limit cycle is not reached in this simulation, the system dissipation must be modified by integrating nonlinearity on the viscoelastic damping parameter of the vortex rope model.

6. NUMERICAL SIMULATION WITH NONLINEAR MODEL PARAMETERS

In this Section nonlinearity of vortex rope model parameters is introduced. The mass flow gain factor is kept as constant whereas the wave speed and the viscoelastic damping are nonlinear. The variation law for the wave speed is derived from CFD simulations whereas the law for the viscoelastic damping is empiric and compared to Eq. 6. Indeed it is difficult task to derive the variation law of the viscoelastic damping which models energy dissipation between liquid and gas from a steady isothermal single phase CFD simulation.

Variation laws of nonlinear parameters

In Section 3 the wave speed has been computed for a given operating point at a given pressure. To derive the variation law of the wave speed as function of pressure, the same methodology is involved by computing the vortex rope volume for several outlet pressure of the computational domain. Therefore, the wave speed is deduced by the derivative of the vortex rope volume as function of the pressure, see Fig. 11.

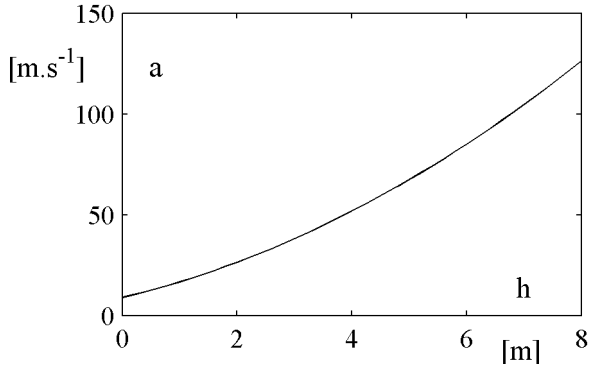

Fig.11 Variation of wave speed as function of pressure

Moreover, an empiric variation law has been derived for the viscoelastic damping parameter to fit time domain simulations with measurements. The proposed model features a variation of the viscoelastic damping proportional to the square of the pressure. The global variation of this parameter is compared to the analytical formulation given by Eq. 6 applied to an ideal gas model. The state equation of an ideal gas being:

$$p \cdot V_c = n \cdot R \cdot T \tag{9}$$

the gas fraction and the wave speed in Eq. 6 can be replaced by the following variation laws:

$$\begin{cases} \alpha_c \sim \dfrac{1}{p} \\ a \sim p \end{cases} \tag{10}$$

Including Eq. 10 in Eq. 6, the analytical variation law as function of pressure is compared to the empiric variation law in Fig. 12.

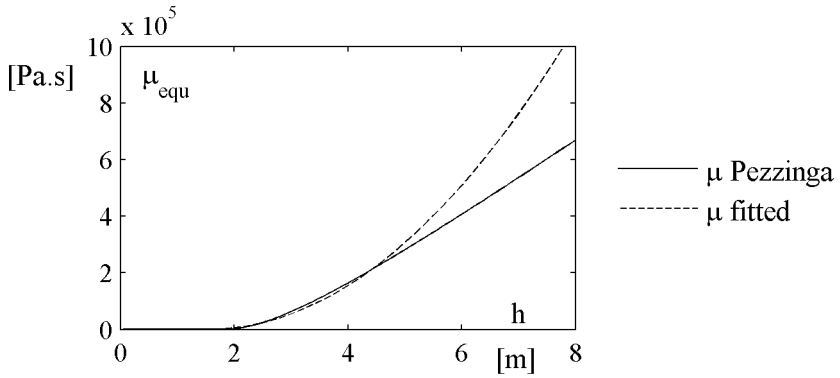

Fig.12 Comparison between the empiric and the analytical variation laws of the viscoelastic damping

For pressure lower than 2 m the equivalent viscoelastic damping is equal to zero corresponding to the situation where the cone and the elbow are filled entirely of gas. Differences between the two variation laws appear at high pressure level.

The variation laws for the wave speed and the viscoelastic damping fit to the set of constant parameters given in Tab. 1 for the pressure in the draft tube corresponding to the operating point.

Time domain simulation

Influence of nonlinearity of each parameter on the time domain simulation is investigated. In Fig. 13 pressure fluctuations of time domain simulations with and without the wave speed nonlinearity are compared.

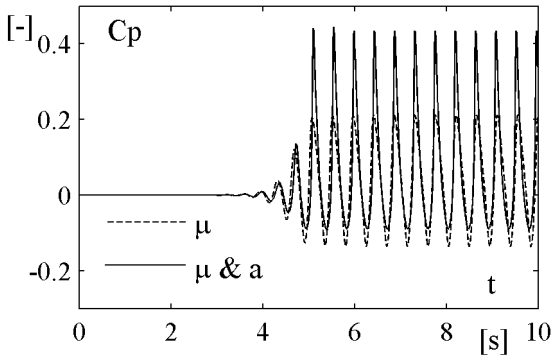

Fig.13 Influence of nonlinearity of each parameter on the time history of pressure fluctuations

One can deduce that the introduction of a nonlinear viscoelastic damping allows to reach the "limit cycle". However, the pressure fluctuations keeps sinusoidal shape whereas experimental data feature a sharped shape for high pressure. By including the nonlinearity of the wave speed the typical researched shape appear with a frequency of $f = 2.7$ Hz. In Fig. 14, inlet and outlet discharges fluctuations of the vortex rope model are compared.

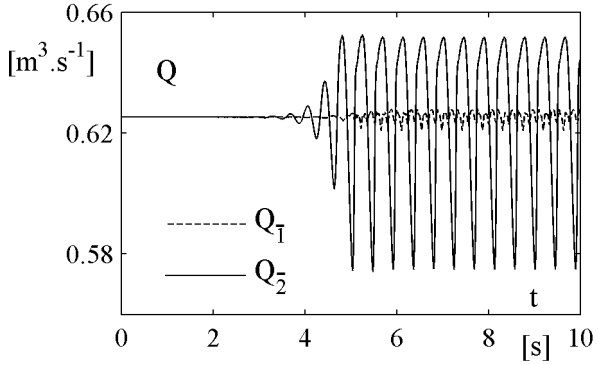

Fig.14 Time history of the inlet and the outlet discharges of the vortex rope model

$Q_{\bar{1}}$ and $Q_{\bar{2}}$ correspond respectively at the upstream and the downstream discharge of the cavitation volume. It shows that during the instability, mass water is moved by the gas volume pulsation. When the vortex rope volume increases, the downstream discharge increases and vice versa. The variation of the viscoelastic damping due to nonlinearity increases dramatically the energy dissipation of the system allowing to reach the "limit cycle" represented in the phase plan in Fig. 15.

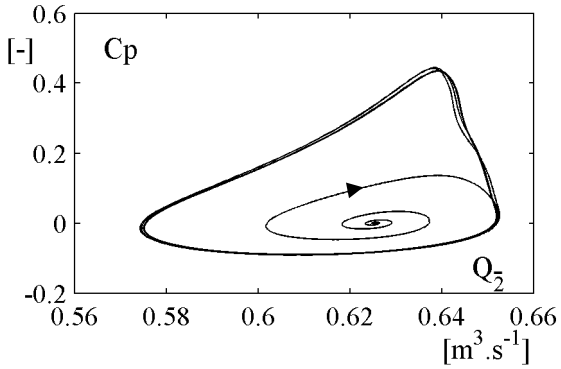

Fig.15 Phase plan representation of the limit cycle

Energy balance during the limit cycle

As introduced in Section 5, during one period of the "limit cycle" represented by the closed path in the phase plan of Fig. 15, the total energy of the system ξ returns to its original value. In the following, an energy balance approach is developed to understand the interaction between the excitation source and the dissipation of the circuit during the limit cycle.

The first step of this approach is to find a formulation of the total energy ξ of the fluid system as function of the state variables of the electrical model. The total energy is constituted of a kinetic energy ξ_k, a potential energy ξ_p and a source energy ξ_s [18]:

$$\xi = \xi_k + \xi_p + \xi_s \tag{11}$$

Considering that the test rig electrical model is divided in n meshes, the total energy of the system is the sum of the energies included in each mesh.

$$\xi = \sum_{i=1}^{n} \xi_i = \sum_{i=1}^{n} \xi_{k_i} + \sum_{i=1}^{n} \xi_{p_i} + \sum_{i=1}^{n} \xi_{s_i} \tag{12}$$

In Fig. 16 a) the mesh including the excitation mass source in the draft tube is given, whereas in Fig. 16 b) a standard mesh is shown.

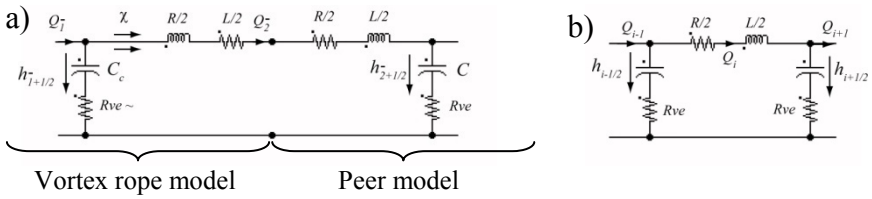

Fig.16 Electrical mesh a) including the excitation mass source and b) without excitation

In the investigated model, the energy source of the excitation is considered only in the mesh given in Fig. 16 a). During the limit cycle this energy can be expressed as:

$$\xi_s = \rho \cdot g \cdot \chi \cdot Q_{\bar{2}} \cdot h_{\bar{1}+1/2} \tag{13}$$

However, for the kinetic and the potential energies, all the meshes must be taken into account. Considering a typical mesh given by Fig. 16 b):

$$\begin{cases} \xi_k = \sum_{i=1}^{n} \xi_{k_i} = \sum_{i=1}^{n} \left(\frac{1}{2} \cdot \rho \cdot g \cdot L \cdot Q_i^2 \right) \\ \xi_p = \sum_{i=1}^{n} \xi_{p_i} = \sum_{i=1}^{n} \left(\int \rho \cdot g \cdot \left(h_{i-1/2} - h_{i+1/2} \right) \cdot Q_i \cdot dt \right) \end{cases} \tag{14}$$

The second step of the approach is to derive the total energy according to the time:

$$\frac{d\xi}{dt} = \sum_{i=1}^{n} \left(\rho \cdot g \cdot Q_i \cdot \left(L \cdot \frac{dQ_i}{dt} + h_{i-1/2} - h_{i+1/2} \right) \right) + \rho \cdot g \cdot \chi \cdot \left(\frac{dQ_{\bar{2}}}{dt} \cdot h_{\bar{1}+1/2} + Q_{\bar{2}} \cdot \frac{dh_{\bar{1}+1/2}}{dt} \right) \tag{15}$$

Using the Kirschoff law applied to the voltages in the mesh given in Fig. 16 b) it yields to:

$$L \cdot \frac{dQ_i}{dt} + h_{i+1/2} - h_{i-1/2} = R_{ve} \cdot \left(Q_{i-1} - Q_i \right) - R_{ve} \left(Q_i - Q_{i+1} \right) + R \cdot Q_i = -H_{l_i} \tag{16}$$

Integrating Eq. 16 in Eq. 15 the derivative of the total energy can be rewritten as:

$$\frac{d\xi}{dt} = -\sum_{i=1}^{n} \left(\rho \cdot g \cdot Q_i \cdot H_{l_i} \right) + \rho \cdot g \cdot \chi \cdot \left(\frac{dQ_{\bar{2}}}{dt} \cdot h_{\bar{1}+1/2} + Q_{\bar{2}} \cdot \frac{dh_{\bar{1}+1/2}}{dt} \right) = \left. \frac{d\xi}{dt} \right|_l + \left. \frac{d\xi}{dt} \right|_s \tag{17}$$

Therefore, the variation of the total energy is due to a balance between the lost power $\left. \frac{d\xi}{dt} \right|_l$ in the resistive components of the electrical circuit and the gain power $\left. \frac{d\xi}{dt} \right|_s$ due to the excitation source. In Fig. 17, time histories of these two powers are plotted.

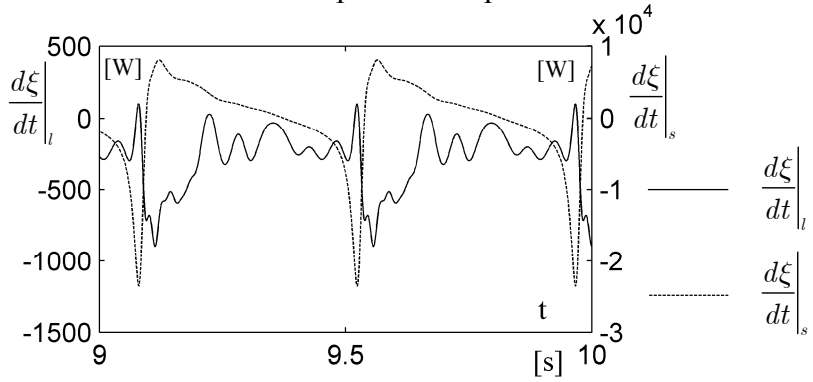

Fig.17 Time histories of the lost power and the gain power

One can observe that during one period, the dissipation can provide energy to the system since the power becomes positive. Hence, in order to balance the total energy, the excitation source dissipates since the power becomes strongly negative. According to Eq. 8, the total energy returns to its original value during a period. According to the previous development Eq. 8 can be rewritten as:

$$\xi(T) - \xi(0) = \int_0^T \frac{d\xi}{dt} \cdot dt = \int_0^T \left. \frac{d\xi}{dt} \right|_l \cdot dt + \int_0^T \left. \frac{d\xi}{dt} \right|_s \cdot dt = 0 \tag{18}.$$

Integrating numerically the two power curves in Fig. 17 over a period, the equality of Eq. 18 is confirmed.

7. CONCLUSION

In this paper a new model for the vortex rope has been developed taking into account an additional dissipation due to thermodynamic exchange between the gas and the surrounding liquid. Therefore three key hydro acoustic parameters must be set up: the compliance or the wave speed, the mass flow gain factor and the additional dissipation called viscoelastic damping. It has been shown that consideration of constant parameters is useful to perform a stability analysis based on eigenvalues and eigenvectors computation. In that case, this linear method allows to identify the stability of the system and to find out unstable frequencies with mode shapes. However, time domain simulation with constant parameters is divergent without reaching a maximum called the "limit cycle". For this reason, nonlinearity of parameters is introduced. It is shown that the essential parameter which allows to reach the limit cycle is the viscoelastic damping. As for the nonlinearity of the wave speed, it allows to reproduce the typical pointed shape of the pressure fluctuations measured on the test rig. Amplitude of the limit cycle is in good agreement with experiments since the variation law of the viscoelastic damping has been fitted to obtain this result. Therefore, futher investigations must be carried out to derive an analytical model for this key parameter. Moreover, an energy approach during the limit cycle showed the interaction process between the excitation mass source of the vortex rope and the system dissipation to reach an equilibrium. Indeed, it brings out that over one period, the dissipation can provide energy to the system whereas the mass source dissipates to ensure the equilibrium.

8. ACKNOWLEDGEMENTS

The authors would like to thank particularly Alstom Power for their financial support and assistance. The project is also financially supported by CTI, the Swiss Federal Comission for Technology and Innovation Grant N° 8330.2 EPRP-IW.

9. REFERENCES

[1] J. KOUTNIK and PULPITEL, L., 1996. *Modelling of the Francis turbine full load surge*. IAHR Symposium on Hydraulic Machinery and Systems, Lausanne.

[2] C. BRENNEN and ACOSTA, A.J., 1973. *Theoretical, quasi static analysis of cavitation compliance in turbopumps*. Journal Spacecraft, Vol 10, p. 175-180.

[3] C. BRENNEN and ACOSTA, A.J., 1976. *The dynamic transfer function for a cavitating inducer*. Journal of fluids engineering ASME, Vol 98, p. 182-191.

[4] Y. TSUJIMOTO, K. KAMIJO and YOSHIDA, Y., 1993. *Theorical analysis of rotating cavitation in inducers*. Journal of fluids engineering, ASME, Vol 115, p. 135-141.

[5] M. DUTTWEILLER and BRENNEN, C., 2002. *Surge instability on a cavitating propeller*. Journal of fluids Mechanics, Vol 458, p. 133-152.

[6] C. BRENNEN and WATANABE, S., 2003. *Dynamics of a cavitating propeller in a water tunnel*. Journal of fluids engineering, ASME, Vol 125, p. 283-292.

[7] F. FLEMMING, J. FOUST, J.Koutnik, R.K. FISHER, 2008. *Overload surge investigation using CFD data*. 24th IAHR Symposium on Hydraulic Machinery and Systems, Foz Do Iguassu.

[8] J. KOUTNIK, C. NICOLET, G.A. SCHOHL and AVELLAN, F., 2006. *Overload surge event in a pumped storage power plant*. IAHR Symposium on Hydraulic Machinery and Systems, Yokohama.

[9] P.S. LANDA, 1996. *Nonlinear oscillations and waves in dynamical systems*. Kluwer Academic Publishers.

[10] A.J. MC MILLAN, 1997. *A nonlinear friction model for self excited vibrations*. Journal of Sound and Vibration, Vol 205, p 323-335.
[11] G. Pezzinga, 2003.*Second viscosity in transient cavitating pipe flows*. Journal of Hydraulic Research, Vol 41, p 656-665.
[12] NICOLET, C.,2007. *Hydroacoustic modelling and numerical simulation of unsteady operation of hydroelectric systems*. PhD thesis, EPFL, Lausanne. N° 3751.
[13] S. ALLIGNE, C. NICOLET, P. ALLENBACH, B. KAWKABANI, J.J. SIMOND, F. AVELLAN, 2008.*Influence of the vortex rope location of a Francis turbine on the hydraulic system stability.* 24th IAHR Symposium on Hydraulic Machinery and Systems, Foz Do Iguassu.
[14] B.W. GRAHAM, 1969. *One dimensional two phase flow.*
[15] H.J. RATH, 1981. *Unsteady pressure waves and shock waves in elastic tubes containing bubbly air water mixtures.* Acta Mechanica, Vol 38, p1-17.
[16] A.P. DOWLING, 1997. *Nonlinear self excited oscillations of a ducted flame.* Journal of Fluid Mechanics, Vol 346, p 271-290.
[17] D.W. JORDAN and P. SMITH, 2007. *Nonlinear ordinary differential equations, an introduction for scientists and engineers.* Oxford University Press.
[18] B.T CHU, 1964. *On the energy transfer to small disturbances in fluid flow (Part I).* Acta Mechanica, p 215-234.

10. NOMENCLATURE

c_p	(-)	pressure coefficient	T	(K)	temperature
p	(Pa)	pressure	n	(mol)	amount of substance
h	(m)	pressure	ξ	(J)	total energy
E	($J.kg^{-1}$)	specific energy	ξ_k	(J)	kinetic energy
H	(m)	net head	ξ_p	(J)	potential energy
Q	($m^3.s^{-1}$)	discharge	ξ_s	(J)	source energy
$Q_{\bar{1}}$	($m^3.s^{-1}$)	discharge inlet vortex rope	R	($s.m^{-2}$)	resistance
$Q_{\bar{2}}$	($m^3.s^{-1}$)	discharge outlet vortex rope	L	($s^2.m^{-2}$)	inductance
σ	(-)	Thoma number	C	(m^2)	capacitance
f	(Hz)	frequency	R_{ve}	($s.m^{-2}$)	viscoelastic resistance
n	(Hz)	rotational frequency			
ρ	($kg.m^{-3}$)	fluid density			
ρ_c	($kg.m^{-3}$)	cavitation density			
ρ_m	($kg.m^{-3}$)	mixture density			
g	($m.s^{-2}$)	gravity acceleration			
A	(m^2)	area			
L	(m)	length			
a	($m.s^{-1}$)	wave speed			
V_c	(m^3)	cavitation volume			
α_c	(-)	fraction volume of cavitation			
C_c	(m^2)	cavitation compliance			
χ	(s)	mass flow gain factor			
μ_{equ}	(Pa.s)	viscoelastic damping			
Θ	(s)	relaxation time			
$\mathscr{R}$	()	constant perfect gas law			